Mon. Not. R. Astron. Soc. **000**, 000–000 (0000) Printed 1 February 2008 (MN LATEX style file v1.4)

The visibility of gamma-ray burst afterglows in dusty star-forming regions

B. P. Venemans[1,2] and A. W. Blain[3]

[1] *Leiden Observatory, P.O. Box 9513, 2300 RA Leiden, The Netherlands*
[2] *Cavendish Laboratory, Madingley Road, Cambridge CB3 0HE*
[3] *Institute of Astronomy, Madingley Road, Cambridge CB3 0HA*

1 February 2008

ABSTRACT

Recent observations of the environments of gamma-ray bursts (GRBs) favour massive stars as their progenitors, which are likely to be surrounded by gas and dust. The visibility of the optical and UV emission of a GRB are expected to depend on the characteristics of both the dust and the GRB emission itself. A reasonable distribution of surrounding dust is capable of absorbing all the optical and UV emission of the optical flash and afterglow of a GRB, unless the optical flash has a peak isotropic luminosity $L_{\rm peak} \gtrsim 10^{49}\,{\rm erg\,s^{-1}}$. This means that dark bursts should exist and these bursts will have to be studied at infrared rather than optical wavelengths. In this paper details will be given about the infrared GRB dust emission. The reprocessed dust emission peaks at a rest-frame wavelength of about $8\,\mu$m. Forthcoming space telescopes, in particular the IRAC camera aboard the *Space Infrared Telescope Facility*, could detect this emission out to a redshift of about 2. However, an accurate position of the GRB afterglow must be provided for this emission to be identified, because the light curve of the reprocessed dust emission does not vary on time-scales less than several years.

Key words: radiative transfer – methods: observational – ISM: clouds – dust, extinction – gamma-rays: burst – infrared: galaxies

1 INTRODUCTION

The first gamma-ray bursts (GRBs), short and intense bursts of $0.1-1\,$MeV photons, were discovered at the end of the 1960s (Klebesadel, Strong & Olsen 1973). In the 1990s the BATSE detector on board the *Compton Gamma-Ray Observatory** observed over 2500 GRBs and showed that GRBs were distributed isotropically over the sky. A suspected conclusion was that GRBs were of extragalactic origin at cosmological distances (see for example Paczynski 1995). This conclusion was confirmed in 1997 using the *BeppoSAX* satellite by the discovery of a well-located transient X-ray counterpart (Costa et al. 1997), and several hours later its association with a fading optical point source (Groot et al. 1997) at a redshift of 0.695 (Sahu et al. 1997). Many more afterglows have now been discovered and more redshifts have been measured (Greiner 2001). Based on the observed gamma-ray flux densities, this implies that the total energy radiated by a GRB is of order 10^{51} to $10^{53}\,$erg, if the emission is isotropic, and is released in a few seconds.

The existence of multi-wavelength afterglows was predicted by models that describe GRBs as opaque radiation-ionized fireballs, generating a relativistic blast wave (e.g. Mészáros & Rees 1993, 1997; Katz 1994); see Piran (1999) for an extensive review of the fireball model. The most promising candidate objects that generate GRBs are binary neutron star mergers (Piran 1999) and hypernovae or collapsars (MacFadyen & Woosley 1999; MacFadyen 2000 and references therein). Observations of the environment in which GRBs occur circumstantially favour massive stars as progenitors of GRBs. For example, multiband photometric imaging of four GRB host galaxies show their that spectral energy distributions (SEDs) are best fitted by starburst spectra (Sokolov et al. 2001). Also, there are some indications from *Hubble Space Telescope* observations that GRB afterglows are associated with bright blue star-forming regions in their host galaxies (for example Bloom et al. 1999b; Fruchter et al. 1999; Bloom, Kulkarni & Djorgovski 2001). The *Infrared Space Observatory* observed the location of a

* see http://cossc.gsfc.nasa.gov/cossc/cgro/batse_src.html

single GRB, GRB970508, both weeks and months after the burst and detected non-transient emission at 60 μm, which was interpreted as an indication of the presence of an ultra-luminous infrared galaxy (ULIRG) (Hanlon et al. 2000). If this ULIRG is the host of the GRB, then the estimated star formation rate must be around 200 $M_\odot\,yr^{-1}$, likely placing this GRB in a very powerful star forming region. Another potentially important discovery, which favours massive stars as progenitors of GRBs, is evidence of a possible supernova component in the afterglow of GRB970228 (Reichart 1999) and GRB980326 (Bloom et al. 1999a). However, an alternative explanation for this, in which scattering of a prompt optical flash by diffuse dust surrounding the GRB explains the observations, has been proposed by Esin & Blandford (2000).

If the progenitors of GRBs are indeed located in star-forming regions, then the GRB is likely to be surrounded by gas and dust. This can influence the spectrum of a GRB, and there have been several recent studies of the effects. Mészáros & Gruzinov (2000) showed that a dense environment should modify the X-ray afterglow of a GRB, flattening the X-ray light curve from hours to days after the burst, before steepening the decay at later times. Waxman & Draine (2000) investigated dust sublimation by GRBs and its implications. They found that a prompt optical flash could destroy up to $10^7\,M_\odot$ of dust out to ~ 10 pc around a GRB. They also calculated that the near-infrared luminosity from dust heated by the optical flash could be as great as $10^{41}\,erg\,s^{-1}$. Perna & Aguirre (2000) proposed to use GRB afterglows as probes of galactic and intergalactic dust. Recently, Galama & Wijers (2001) found high X-ray absorption column densities, but low optical extinctions for their sample of GRB afterglows. They inferred that most GRBs are embedded in large molecular clouds, and are therefore likely to be produced by the death of short-lived massive stars, but that the surrounding dust is destroyed by hard radiation from the GRB, leaving the afterglow unextinguished.

In this article, the influence of surrounding dust on the visibility of the afterglow and optical flash of a GRB is investigated in order to study if such luminous events could be detected at high redshift, even if they occur in dense dusty environments. The interaction of homogeneously distributed dust around a GRB with the optical and UV emission of the burst afterglow is modelled. The unextinguished light curve of a GRB is described in section 2. A dust model consisting of carbon grains with a range of sizes is used, which takes account of the evolution of opacity, dust sublimation and temperature; see section 3. The model is used to estimate both the visibility of the optical/UV afterglow for different densities and profiles of the surrounding dust (section 4), and the properties of the thermal emission of this dust (section 5). Finally the flux densities of the dust emission are compared with the sensitivity of future infrared detectors (section 6).

2 GRB OPTICAL LIGHT CURVES

The optical light curve of a typical GRB consists of two parts: a prompt optical flash coincident with the gamma-ray emission and a late-time afterglow. The afterglow can be explained by synchrotron emission from a decelerating relativistic shell in collision with an external medium: see Sari, Piran & Narayan (1998) for an analytical description of the light curve or Piran (1999) for a more detailed derivation.

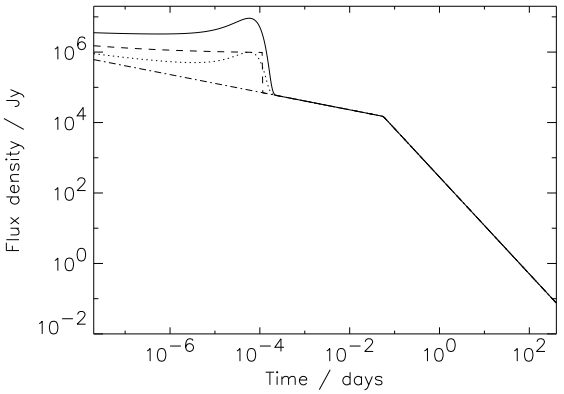

Figure 1. B–band flux densities 1 Mpc away from a GRB with a light curve described by the model of Sari et al. (1998) used here. An afterglow with a Gaussian optical flash with $L_{peak} = 10^{49}\,erg\,s^{-1}$ in the energy range $h\nu = 1 - 7.5$ eV is shown by the solid curve; one with a Gaussian optical flash with $L_{peak} = 10^{48}\,erg\,s^{-1}$ is shown by the dashed curve; an afterglow without an optical flash is shown by the dot–dashed curve; and an afterglow with a top-hat optical flash with $L_{peak} = 10^{48}\,erg\,s^{-1}$ is shown by the dotted curve.

We assume that the peak frequency of the optical flash falls in the optical waveband (Sari & Piran 1999), and that the time profile of the optical flash is represented as either a Gaussian or a top-hat function. Both the peak luminosity and the duration of the flash are left as free parameters, but typical values of the peak luminosity are $L_\nu = 0.5 - 5 \times 10^{33}\,erg\,s^{-1}\,Hz^{-1}$ at a frequency $\nu = 1.4 \times 10^{15}$ Hz, with a SED $L_\nu \propto \nu^{-1/2}$ and a duration of order 10 s (Akerlof et al. 1999; Waxman & Draine 2000).

Waxman & Draine (2000) showed that photons in the energy range $1 - 7.5$ eV will dominate the heating of the dust, as in dense regions (typically with hydrogen column densities $n_H \gtrsim 10^2\,cm^{-3}$) photons with energy $h\nu > 13.6$ eV will photoionize hydrogen very efficiently, while $7.5 - 13.6$ eV photons can be efficiently absorbed by H_2, by either vibrational excitation or photodissociation (see also Draine 2000). The number of photons at $h\nu > 7.5$ eV that are available for dust heating will thus probably be negligible. The lower limit of 1 eV is taken because both the fraction of the energy radiated by the GRB below this energy is small and the absorption efficiency of dust decreases rapidly at wavelengths longer than about 1 μm ($\equiv 1.24$ eV) (Draine & Lee 1984).

The following parameters are used to describe the afterglow, based on values derived from observations (including Galama et al. 1999a; Lamb, Castander & Reichart 1999; Huang, Dai & Lu 2000; Greiner 2001). The energy of the shell $E = 5 \times 10^{52}$ erg, the fraction of the shell energy that goes into the kinetic energy of electrons $\epsilon_e = 0.15$, the ratio of the magnetic field energy density to the total thermal energy $\epsilon_B = 0.1$, the surrounding density $n_1 = 5 \times 10^3\,cm^{-3}$ and the coefficient of the power-law distribution of electron energies in the GRB shell $p = 2.5$. The hydrodynamic evolution

of the shock is assumed to be adiabatic, because radiative evolution only applies if $\epsilon_e \simeq 1$.

In Fig. 1 four different optical light curves of GRBs, used in our model, are plotted.

3 RADIATION ABSORPTION AND EMISSION BY DUST GRAINS

3.1 Dust temperature

The temperature of dust determines its emission spectrum. Because the GRB afterglow is very luminous, the influence of heating by both reprocessed dust emission from within the dust cloud and background radiation from the interstellar radiation field of the galaxy can generally be neglected. The dust grains are assumed to be spherical with a radius a. A source of radiation with a luminosity $L = \int L_\nu \mathrm{d}\nu$ is at a distance r from a dust grain. If the temperature of a dust grain is less than the temperature at which sublimation is a more efficient energy loss mechanism than radiation, then the dust temperature T_d can be calculated using

$$\pi a^2 \frac{L}{4\pi r^2}\overline{Q_\mathrm{abs}}(a) = 4\pi a^2\ Q_\mathrm{em}(a,T_\mathrm{d})\sigma T_\mathrm{d}^4 + \frac{4}{3}\pi a^3\ C_\mathrm{V}\frac{\mathrm{d}T_\mathrm{d}}{\mathrm{d}t} \tag{1}$$

(all the equations in this section are adapted from Draine & Lee 1984, Siebenmorgen, Krügel & Mathis 1992, Evans 1993 and Waxman & Draine 2000). $\overline{Q_\mathrm{abs}}$ is the weighted effective absorption efficiency, σ is the Stefan-Boltzmann constant, C_V is the specific heat capacity and Q_em is the Planck-averaged emission efficiency,

$$Q_\mathrm{em}(a,T) \equiv \frac{\int B_\nu(T) Q_{\nu,\mathrm{abs}}(a)\mathrm{d}\nu}{\int B_\nu(T)\mathrm{d}\nu}. \tag{2}$$

The weighted effective absorption efficiency

$$\overline{Q_\mathrm{abs}} = \frac{\int_0^\infty\ L_\nu Q_{\nu,\mathrm{abs}}\ \mathrm{d}\nu}{\int_0^\infty\ L_\nu\ \mathrm{d}\nu}, \tag{3}$$

depends on the spectrum of the source.

When subjected to very intense radiation from the optical flash of a GRB, the temperature of dust can rise to levels where cooling of the grains by sublimation is the dominant cooling process.

The cooling rate due to sublimation of a spherical dust grain per unit time, $\dot{E}_\mathrm{sub}$,

$$\dot{E}_\mathrm{sub} = 4\pi a^2 \frac{\rho}{m} B \frac{\mathrm{d}a}{\mathrm{d}t} \tag{4}$$

can be described in terms of the reduction in the grain radius, $\mathrm{d}a/\mathrm{d}t$, where ρ is the mass density of the grain, m the mean atomic mass and B is the chemical binding energy per atom within a grain. An approximation to the sublimation rate, $\mathrm{d}a/\mathrm{d}t$, is given by

$$\frac{\mathrm{d}a}{\mathrm{d}t} = -\frac{P_0 e^{-T_0/T(t)}}{\rho}\left(\frac{m}{2\pi kT}\right)^{1/2}. \tag{5}$$

P_0 and T_0 are constants, which depend on the properties of the grain material.

Now, using equation (1) and including the sublimation, equation (4), the out-of-equilibrium temperature T_d of a dust grain can be calculated using

$$\pi a^2\ \frac{e^{-\tau}\ L}{4\pi r^2}\overline{Q_\mathrm{abs}}(a) = 4\pi a^2\ Q_\mathrm{em}\left(a,T_\mathrm{d}\right)\sigma T_\mathrm{d}^4 - 4\pi a^2\ \frac{\rho}{m}B\frac{\mathrm{d}a}{\mathrm{d}t} + \frac{4}{3}\pi a^3\ C_\mathrm{V}\frac{\mathrm{d}T_\mathrm{d}}{\mathrm{d}t}, \tag{6}$$

in which τ is the optical depth between the source and the dust grain (described in more detail in section 3.3). Equation (6) has the same structure as equation (8) of Waxman & Draine (2000), but with a term included for the heat capacity, which can be important at temperatures below the sublimation temperature, where thermal emission is the most important cooling mechanism.

Equations (5) and (6) are coupled differential equations for the evolution of the temperature $T_d(t)$ and radius $a(t)$ of a dust grain.

The period of time during which a grain is entirely sublimated after the arrival of a GRB afterglow is defined as the destruction time and is, in general, a function of both grain size and distance to the source: $t_\mathrm{des} = t_\mathrm{des}(a,r)$.

3.2 Dust luminosity

The luminosity of a single dust grain is

$$L_\mathrm{d}(a,t) = 4\pi a(t)^2 Q_\mathrm{em}\left[a(t),T(t)\right]\sigma T(t)^4 \tag{7}$$

assuming the grain radiates as a modified blackbody with an emission efficiency Q_em (equation 2).

The flux density received a distance r from a grain, that is radiated in a frequency band between ν_min and ν_max, can now be calculated. Defining $x_\mathrm{min} = h\nu_\mathrm{min}/kT(t)$ and $x_\mathrm{max} = h\nu_\mathrm{max}/kT(t)$, the flux at a distance r from a single grain is approximately

$$F(a,t) = \frac{1.9\times10^{-2}\ L_\mathrm{d}(a,t)}{4\pi r^2}\ \int_{x_\mathrm{min}}^{x_\mathrm{max}} \frac{x'^{4.5}}{e^{x'}-1}\,\mathrm{d}x', \tag{8}$$

assuming a reasonable emissivity index β of 1.5, where $\epsilon_\nu\ \propto\ \nu^\beta$. To calculate the evolution of the flux of a shell with radius R consisting of grains with size a, the flux of all the grains must be added, taking into account the time delay due to the differences in distance from the individual grains in the shell to the observer. A photon emitted by a grain at an angle θ from the line of sight has to travel an extra distance of $R\left(1-\cos\theta\right)$ as compared with a photon emitted from the same shell at the same time, but directly along the line of sight in order to be detected simultaneously by the same observer. If we assume that the distance to the observer is much greater than the radius of the shell ($r \gg R$), and the number density of grains is n, then the total flux received by the observer is the integral over all shells:

$$F_{\rm tot}(t) = \int_a \int_R F(R,a,t)\,{\rm d}R\,{\rm d}a = \int_a \int_R \int_\theta 2\pi R^2\, n(R,a)\sin\theta\, F[a, t+\frac{R}{c}(\cos\theta - 1)]\,{\rm d}\theta\,{\rm d}R\,{\rm d}a. \quad (9)$$

Equation (9) can only be used for calculating the dust emission in the case of a spherical distribution of dust around a GRB, the emission from which is itself isotropic. If, for example, the afterglow emission of the GRB is beamed, then (roughly) only the dust inside the opening angle θ_0 of the beam will be heated. In that case, the emission will be reduced by $\sim \theta_0^2/4$, and the time profile of the dust radiation will change, depending on both the opening angle and inclination of the beam to the line of sight. Recently, Frail et al. (2001) derived opening angles of GRBs by analysing gradient changes in the multicolour light curves of GRB afterglows. They concluded that the afterglow emission of GRBs is generally beamed, with values for θ_0 ranging between 0.05 and 0.4 radians. This could hence be an important effect, significantly reducing the intensity of the infrared radiation emitted from a reprocessed afterglow as compared with the predictions in the isotropic model presented here.

In a preprint pointed out by the referee, Fruchter, Krolik & Rhoads (2001) discuss dust destruction by X-rays. They found that heating by the optical/UV flash and by X-rays have roughly comparable importance for grain evaporation, and either may be more important, depending on the burst spectrum and grain size distribution. Optical/UV heating is generally more important for small grains and X-ray heating for large grains, although the division depends on grain composition. They also found that under most circumstances grain charging and electrostatic shattering is a more effective mechanism in destroying dust grains, compared to heating and evaporation, in disagreement with the conclusions of Waxman & Draine (2000), who found that grain shattering does not appreciably reduce the UV/optical extinction. The processes described by Fruchter et al. (2001) could reduce the number of dust grains surrounding a GRB, and so further reduce the infrared dust emission.

If the distribution of the dust is not homogeneous but clumpy, then the heating of a dust grain will not only depend on R but also on θ and ϕ ($F = F[R,a,t,\theta,\phi]$) and equation 9 will no longer be valid. At some places, radiation levels inside the clumpy medium are greatly enhanced with respect to a homogeneous medium due to relatively dust-free lines of sight, while at other places radiation levels are lower due to more effective screening (for example, see Hobson & Padman 1993; Hobson & Scheuer 1993).

3.3 Optical depth

Assume a source of radiation is surrounded by spherical shells of dust. The optical/UV flux from the source incident on a dust grain at a given radius from the source will be attenuated by the dust at smaller radii, and so the optical depth, τ, between the source and the grain will be non zero. In general, τ_ν is defined as

$$\tau_\nu = \int_r \kappa_\nu\ {\rm d}r = \int_r \int_a n(a,r)\sigma_\nu(a)\ {\rm d}a\,{\rm d}r \quad (10)$$

where $\sigma_\nu(a)$ is the absorption cross-section of a dust grain with size a and $n(a,r)$ is the number density of dust grains with sizes between a and $a + {\rm d}a$ at a distance r from the GRB. Because some of the dust grains can be sublimated due to intense heating from the source, τ_ν will in general also be a function of time. The absorption cross section is

$$\sigma_\nu(a,r,t) = \begin{cases} Q_{\nu,{\rm abs}}(a)\pi a^2, & t < t_{\rm des}(a,r) \\ 0, & t > t_{\rm des}(a,r), \end{cases} \quad (11)$$

where $t_{\rm des}(a,r)$ is the destruction time of a grain with size a at a distance r from the source and $Q_{\nu,{\rm abs}}(a)$ the absorption coefficient. To compute κ_ν an expression for $n(a,r)$ is required. In this model the empirical law

$$n(a,r) = C(r)a^{-3.5} \quad (12)$$

(Mathis, Rumpl & Nordsieck 1977; Hildebrand 1983) was used for the grain size distribution, in which

$$C(r) = \frac{3\ n_{\rm H}(r)\ m_{\rm H}}{8\pi\rho\, M_{\rm g}/M_{\rm d}\ (\sqrt{a_{\rm max}} - \sqrt{a_{\rm min}})}. \quad (13)$$

$n_{\rm H}(r)$ is the number density of neutral hydrogen, $m_{\rm H}$ is the atomic mass of hydrogen, $M_{\rm g}/M_{\rm d}$ is the gas-to-dust mass ratio, ρ is the mean mass density of the dust grains, and $a_{\rm min}$ and $a_{\rm max}$ are the minimum and maximum grain radii.

Using equations (10) to (13), the total optical depth can now be calculated. This is the optical depth due to dust immediately surrounding the GRB. In addition, an afterglow light curve can be attenuated by dust along the line of sight within the host galaxy of the burst, in the intergalactic medium (Perna & Aguirre 2000) and in our own galaxy.

With the expressions for the light curve of GRB afterglows with or without an optical flash (see section 2 above), the luminosity in the photon energy range $h\nu = 1 - 7.5\,{\rm eV}$, $L_{1-7.5}(t)$, can now be calculated, and so the dust properties $T(t)$, $\tau(r,t)$ and $a(t)$ can be computed throughout the enshrouding dust cloud, as the optical emission of the GRB travels through it.

3.4 Numerical model

3.4.1 Grain material

For the simulations a model of dust consisting of carbon grains with various sizes was used. Graphite grains are better absorbers of optical and UV photons than silicate grains (Mezger, Mathis & Panagia 1982; Draine & Lee 1984). On the other hand, silicate grains are destroyed at lower temperatures than graphite grains because their chemical bonds are weaker (Guhathakurta & Draine 1989; Evans 1993). Graphite grains will thus get hotter, but are also more robust, and so the destruction time of graphites and silicates are not expected to differ by large factors. Hence, because of their higher absorptivity, graphite grains are likely to dominate the optical depth at optical and UV wavelengths.

3.4.2 Absorption and emission coefficients

The value of the absorption coefficient of a graphite grain in the energy range $1 - 7.5\,\mathrm{eV}$, $\overline{Q_{\mathrm{abs}}}$, depends on the grain size. Based on the results of computations by Draine & Lee (1984), if we define an effective wavelength λ_{eff} to account for the interaction of the physical properties of the grains and the illuminating radiation field, then the absorption coefficient

$$\overline{Q_{\mathrm{abs}}}(a) = \begin{cases} 10\,a\,\lambda_{\mathrm{eff}}^{-1}, & a < 0.1\,\lambda_{\mathrm{eff}} \\ 1, & a > 0.1\,\lambda_{\mathrm{eff}}. \end{cases} \qquad (14)$$

A value of $0.5\,\mu$m is taken for λ_{eff}, because in the GRB afterglow model approximately half the energy is radiated at longer wavelengths and half at shorter wavelengths, depending on whether or not there is an optical flash, which is expected to be bluer than a typical afterglow. Changing λ_{eff} from $0.4\,\mu$m to $0.6\,\mu$m made little difference to the outcome of the simulations: the destruction time of the grains and the dust emission both changed by only about 1 per cent. Empirical values from Draine (2001) were taken for the emission coefficients, Q_{em} (equation 2).

3.4.3 Density profiles and dust mass

Two different dust density profiles were considered; a constant density at all radii and an isothermal density profile, that is $n(r) \propto r^{-2}$. A gas-to-dust mass ratio of 10^2 was assumed (Hildebrand 1983; Evans 1993). In the model it is assumed there is no dust within 0.3 pc of the GRB. This is the Strömgren radius of an HII region with $n_{\mathrm{H}} = 5000\,\mathrm{cm}^{-3}$ surrounding a star of spectral type O6. If the progenitors of GRBs are massive stars of this type, then it is unlikely that significant amounts of dust will be able to survive within the Strömgren sphere. Assuming a different inner radius, however, does not affect the optical depth or the dust mass strongly. Even if the inner radius is reduced to zero, then the dust mass will change by only a few percent. The maximum radius is taken to be 3.67 pc and 10.33 pc in the case of a constant and isothermal density profile respectively. The total dust mass is $0.234\,(n_{\mathrm{H}_{0.3}}/\mathrm{cm}^{-3})\,\mathrm{M}_\odot$ and $0.016\,(n_{\mathrm{H}_{0.3}}/\mathrm{cm}^{-3})\,\mathrm{M}_\odot$ in these cases respectively, where the density of hydrogen at 0.3 pc ($n_{\mathrm{H}_{0.3}}$) is a free parameter in the model.

3.4.4 Minimum and maximum grain size

As mentioned in section 3.3 an empirical law (equation 12) was used for the distribution of dust grain sizes from $0.005\,\mu$m (a_{min}) to $2.5\,\mu$m (a_{max}). The minimum grain size was derived by Mathis et al. (1977). The maximum grain size is adopted from Witt, Oliveri & Schild (1990) and Aitken et al. (1993). However, the maximum grain size assumed by different authors varies widely, in papers about theory as well as in papers about observations. To investigate the effect of the minimum and maximum value of the grain size on the results of the dust model, the range was extended to $0.001\,\mu$m as a lower limit, to reach molecular sizes, and to $5\,\mu$m as an upper limit.

The upper limit to the grain size has the strongest influence on the total number of dust grains for a fixed dust mass in the model, because the maximum grain size determines the value of $C(r)$ (equation 13). If the maximum size of the grains is increased by a factor of 2, then the value of $C(r)$ will decrease by a factor of approximately $\sqrt{2}$. This influences both the optical depth and the dust luminosity; for example, for the same total dust mass, the decrease in the number of small grains as a_{max} increases will lead to a reduction in the optical depth, because the optical depth is dominated by smaller grains that are still larger than molecules (see equation 11: $\mathrm{d}\tau \sim a^{-1.5}\,\mathrm{d}a$), as shown in Table 1. Hence, the choice of maximum grain size has a significant effect, because it determines the number of dust grains. However, if $C(r)$, and thus the number of grains with a given radius, is kept fixed, then neither the optical depth nor the dust emission change significantly as a function of a_{max}: the change in dust emission with a_{max} is less than 1 per cent at all wavelengths. The effect of changing the upper limit of grain size in the model is thus negligible if the normalization of $n(a, r)$ is kept constant, although the total mass of dust will then change.

Decreasing the lower limit of the grain size from $0.005\,\mu$m to $0.001\,\mu$m with $n_{\mathrm{H}_{0.3}}$ fixed increases the optical depth by about 11 per cent (see Table 1), while $C(r)$ only changes by about 2 per cent. Because of the increased amount of energy absorbed by the smallest grains when a_{min} is reduced, the optical/UV flux density of the late-time afterglow is also reduced by 40 per cent. However, the dust luminosity does not change by a large amount, because the fractional change in the amount of energy absorbed is only of order 0.1 per cent. Decreasing the minimum grain size further has a negligible effect on both the dust emission and the optical depth, as the additional amount of energy absorbed is very small.

Absorption by large molecules or Polycyclic Aromatic Hydrocarbon maolecules (PAHs) only become an important factor for the optical depth at photon energies $h\nu \gtrsim 10\,\mathrm{eV}$, at which their absorption cross sections increase to be comparable to their physical cross section (Draine & Lee 1984). Below those photon energies, the optical depth is dominated by bigger grains (see also Désert, Boulanger & Puget 1990). Because photons with energy $h\nu > 7.5\,\mathrm{eV}$ will mainly be

Table 1. Optical depth all the way through the dust cloud for different profiles and limits of grain sizes. The total dust mass and maximum radius in the case of a flat density profile is $0.234\,(n_{\mathrm{H}_{0.3}}/\mathrm{cm}^{-3})\,\mathrm{M}_\odot$ and 3.67 pc. In the case of decreasing profile these are $0.016\,(n_{\mathrm{H}_{0.3}}/\mathrm{cm}^{-3})\,\mathrm{M}_\odot$ and 10.33 pc. To calculate the optical depth at other wavelengths, it is assumed that the optical depth varies as $\propto \lambda^{-1}$ at wavelengths $0.5\,\mu\mathrm{m} < \lambda < 1.25\,\mu\mathrm{m}$ (for example, Evans 1993) and as $\propto \lambda^{-1.6}$ at wavelengths $\lambda > 1.25\,\mu$m (Cardilli, Clayton & Mathis 1989; Mathis 1990).

profile	$a_{\mathrm{min}}/\mathrm{cm}$	$a_{\mathrm{max}}/\mathrm{cm}$	$\tau(\lambda = 0.5\,\mu\mathrm{m})/\mathrm{cm}^{-3}$
flat $\propto r^0$	5×10^{-7}	2.5×10^{-4}	$2.8\times10^{-3}\ n_{\mathrm{H}_{0.3}}$
	10^{-7}	2.5×10^{-4}	$3.1\times10^{-3}\ n_{\mathrm{H}_{0.3}}$
	5×10^{-7}	5×10^{-4}	$1.8\times10^{-3}\ n_{\mathrm{H}_{0.3}}$
isothermal $\propto r^{-2}$	5×10^{-7}	2.5×10^{-4}	$2.6\times10^{-4}\ n_{\mathrm{H}_{0.3}}$
	10^{-7}	2.5×10^{-4}	$2.9\times10^{-4}\ n_{\mathrm{H}_{0.3}}$
	5×10^{-7}	5×10^{-4}	$1.7\times10^{-4}\ n_{\mathrm{H}_{0.3}}$

Table 2. Values of some important parameters, used for simulations. In the table OF is the representation of the optical flash (e.g. Gaussian), $L_{\rm peak}$ is the peak luminosity of the optical flash in the energy band $1-7.5\,{\rm eV}$ in ${\rm erg\,s^{-1}}$ and profile is the density profile. The duration of the optical flash is in each case 10 s. In Fig. 1 the unattenuated light curves are plotted.

light curve	$L_{\rm peak}$	$n_{\rm H}/{\rm cm^{-3}}$	profile	name
Gaussian OF + afterglow	10^{49}	5×10^3	flat	A_1
		5×10^4	flat	A_2
		5×10^3	isothermal	A_3
		5×10^4	isothermal	A_4
		5×10^5	isothermal	A_5
Gaussian OF + afterglow	10^{48}	5×10^3	flat	B_1
		5×10^4	flat	B_2
		5×10^3	isothermal	B_3
		5×10^4	isothermal	B_4
		5×10^5	isothermal	B_5
afterglow only	–	5×10^3	flat	C_1
		5×10^4	flat	C_2
		5×10^3	isothermal	C_3
		5×10^4	isothermal	C_4
		5×10^5	isothermal	C_5
Top hat OF + afterglow	10^{48}	5×10^5	isothermal	D

absorbed both by H and H_2 in the early phases of the GRB (Waxman & Draine 2000, see section 2), the smallest grains and molecules are unlikely to contribute significantly to the total dust emission.

The minimum and maximum grain sizes used in the model were assumed to be $0.005\,\mu$m and $2.5\,\mu$m respectively. However, changing the minimum and maximum grain size was found not to influence the results of the model significantly, if the number of grains with a given radius was kept fixed.

4 RESULTS: OPTICAL LIGHT CURVES

In Table 2 the parameters describing the light curves and the properties of surrounding dust clouds used here are listed. In Fig. 2a light curves are plotted for a GRB with an afterglow and an optical flash with a peak luminosity of $10^{49}\,{\rm erg\,s^{-1}}$ as it would appear to an observer at a distance of 1 Mpc, including the effects of absorption by dust surrounding the GRB.

As can be seen in Fig. 2a, the optical flash is able to destroy large amounts of dust. Although the total dust mass in the cloud varies a great deal from model to model (see section 3.4), and can be as great as $2300\,{\rm M_\odot}$, the visibility of the afterglow is hardly reduced after the first few seconds. In the case of a flat dust density profile with $n_{\rm H}=0.5$ and $5{\times}10^4\,{\rm cm^{-3}}$, as represented by curve A_1 and A_2 respectively, all the dust is destroyed by the optical flash and observations of the afterglow would not reveal any dust surrounding the GRB. In the case of an isothermal density profile, some of the bigger dust grains in the outer shells survive the passage of the flash. This is not because of screening by the absorption due to grains at smaller radii, but because the distance to the burst is sufficiently large that the intensity of the op-

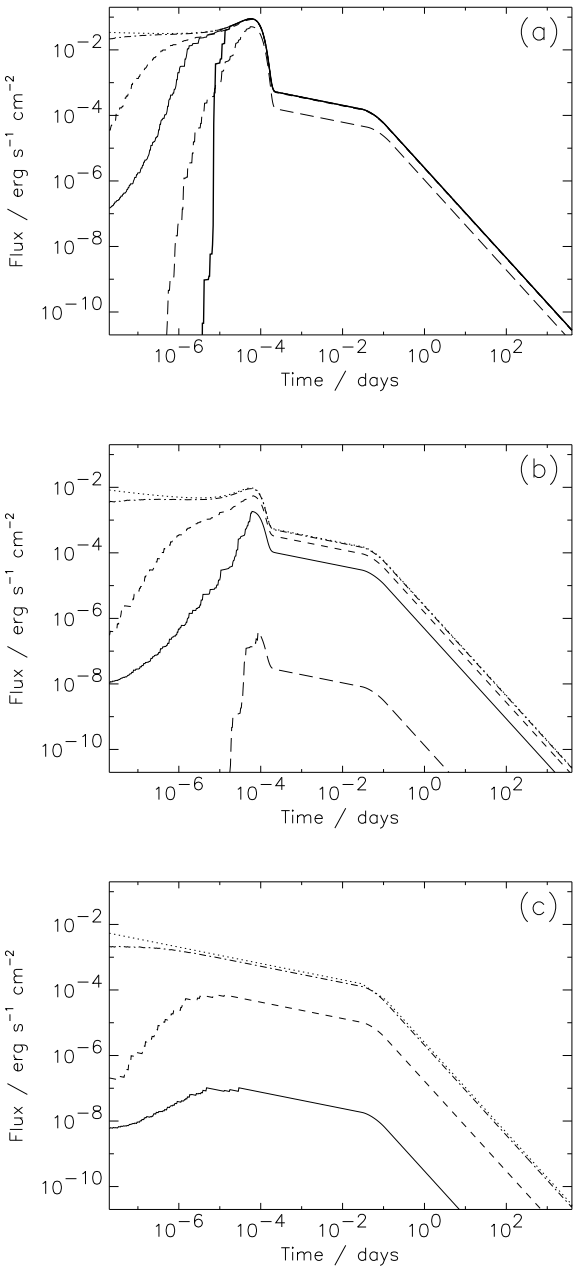

Figure 2. (a) Integrated flux of a GRB afterglow plus a Gaussian optical flash with $\rm L_{peak}=10^{49}\,erg\,s^{-1}$ at a distance of 1 Mpc between $\nu=2.4\times10^{14}\,$Hz and $\nu=1.8\times10^{15}\,$Hz. The dotted line is the light curve with no extinction. The thin solid line and the thick solid line include absorption by dust with a flat density profile and a density of $n_{\rm H}=0.5$ and $5\times10^4\,{\rm cm^{-3}}$ respectively (light curve A_1 and A_2 of Table 2). The dash-dotted line, the dashed line and the long-dashed line include absorption by dust with an isothermal density profile and a maximum density of $n_{\rm H,max}=0.5$, 5 and $50\times10^4\,{\rm cm^{-3}}$ respectively (light curve A_3, A_4 and A_5 of Table 2). (b) As (a), but with an optical flash with $\rm L_{peak}=10^{48}\,erg\,s^{-1}$. The light curve which includes absorption by dust with constant density of $n_{\rm H}=5\times10^4\,{\rm cm^{-3}}$ (light curve B_2) is not shown, because the flux is close to zero because of the very powerful absorption in this case. (c) As (a), but with no optical flash. Light curves C_2 and C_5 are not shown, because the flux is almost zero due to absorption by the dust.

tical/UV flux has decreased below the level at which grains are destroyed by sublimation. For example, beyond about 4.5 pc the flux density of even an unattenuated flash with a peak luminosity of $10^{49}\,\mathrm{erg\,s^{-1}}$ is not sufficient to sublime the largest grains ($a \gtrsim 1\,\mu\mathrm{m}$).

When the peak of the optical flash is less intense, $10^{48}\,\mathrm{erg\,s^{-1}}$, less dust is destroyed along the line of sight, and so the afterglow is attenuated to a greater degree (see Fig. 2b). In the case of a flat profile with $n_\mathrm{H} = 5\times10^4\,\mathrm{cm^{-3}}$, practically all the optical/UV energy of the flash and afterglow is absorbed by the surrounding dust. In the case of an isothermal profile and a density of $n_\mathrm{H} = 5\times10^5\,\mathrm{cm^{-3}}$, the afterglow is attenuated by a factor of about 2.5×10^5 or 11 magnitudes. Hence, it is very unlikely that an optical/UV afterglow would be detected; for example, the unattenuated R-band magnitude of a GRB afterglow at a relatively low redshift $z = 0.3$ one day after the start of the burst, which is predicted to be $R \sim 18$, would be reduced to $R \sim 29$.

In the densest environments, the afterglow of a GRB with a relatively weak optical flash will be heavily attenuated; however, in less dense environments, such a burst will only be marginally affected.

If there is no optical flash (or if the intensity of the optical flash has an insignificant value of $L_\mathrm{peak} \lesssim 10^{47}\,\mathrm{erg\,s^{-1}}$), then almost no dust is destroyed, and so the optical/UV afterglow emission from the GRB will be severely attenuated in all cases: see Fig. 2c. If the shape of the optical flash is a top-hat and not a Gaussian, then more dust will be destroyed, simply because there is more energy in a flash with a top-hat profile than in a Gaussian flash with the same peak flux.

In conclusion, the higher the peak luminosity of the optical flash, the greater is the amount of dust that is expected to be destroyed in the environment of the GRB, and so the afterglow will be less attenuated. If the peak luminosity of the optical flash is $\gtrsim 10^{49}\,\mathrm{erg\,s^{-1}}$, then the intensity of the afterglow emission will never be reduced significantly. If the peak luminosity of the optical flash $\lesssim 10^{47}\,\mathrm{erg\,s^{-1}}$, then the afterglow will always be highly obscured, unless the total mass of the dust within a few pc surrounding the GRB is less than $100\,\mathrm{M_\odot}$, which would be the case for $n_\mathrm{H} \lesssim 10^3\,\mathrm{cm^{-3}}$ and a gas-to-dust mass ratio of about 10^2.

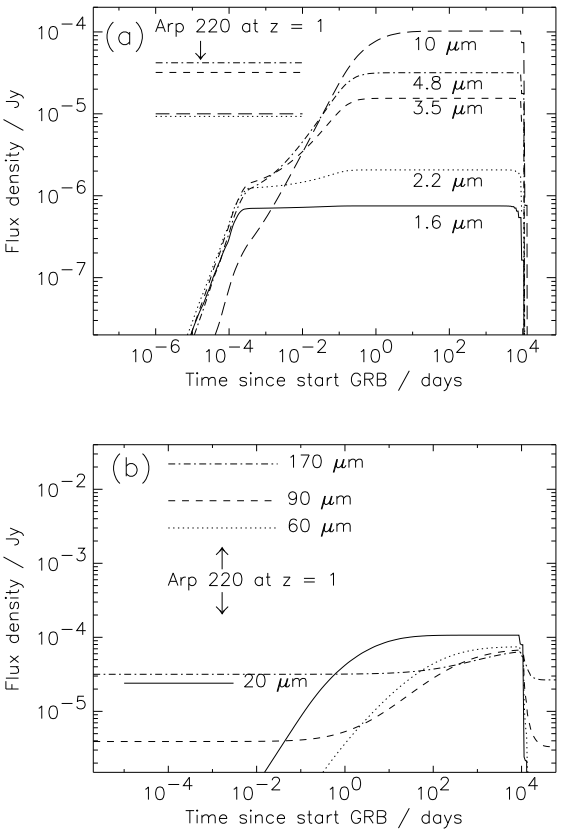

Figure 3. (a) Emission from dust surrounding a GRB at $z = 1$. Light curve B_2, which is described in Table 2, was assumed to heat the dust, which absorbed all the energy of the light curve as shown in Fig. 2b. Here the reprocessed emission at observed wavelengths of 1.6, 2.2, 3.5, 4.8 and 10 μm are plotted. (b) The corresponding emission at four longer observed wavelengths of 20, 60, 90 and 170 μm. In both figures the flux densities at the same wavelengths of the luminous dusty star-forming galaxy Arp 220, redshifted to $z = 1$, are shown for comparison.

5 RESULTS: DUST EMISSION

5.1 Dust emission from the GRB environment

The dust emission observed from around a GRB at a given wavelength depends on the density and profile of the surrounding dust, the peak luminosity of the optical flash, the light curve of the GRB afterglow and the redshift of the GRB. To illustrate the key properties of the dust emission, a single optimistic set of model parameters was assumed. The density profile of the dust was assumed to be flat with $n_\mathrm{H} = 10^4\,\mathrm{cm^{-3}}$. The GRB optical/UV light curve was assumed to be B_2 in Table 2. The redshift of the GRB was assumed to be $z = 1$, corresponding to a luminosity distance $d_\mathrm{L} = 5.4\,\mathrm{Gpc}$ ($H_0 = 65\,\mathrm{km\,s^{-1}\,Mpc^{-1}}$ and $q_0 = 0.5$). The GRB emission was assumed to be isotropic, not beamed. This optimistic set of parameters also ensures an intense dust emission signal – more than $2400\,\mathrm{M_\odot}$ of dust surrounds the GRB, and nearly all the energy of the afterglow and optical flash is absorbed and re-emitted by the dust. In Fig. 3 the associated dust emission predicted by the radiative transfer model at eight observed wavelengths between 1.6 μm and 170 μm is plotted. A characteristic feature of the emission from the spherical distribution of dust in this case is that the detected signal is a top-hat function. The emission at the high-energy end of the dust radiation spectrum is radiated predominantly by hot grains near their sublimation temperature in the time before they vaporize. These grains are located close to the GRB, at a distance $R \sim 1\,\mathrm{pc}$. Because these grains are vaporized by the intense radiation of the optical flash, the dust emission at short wavelengths starts to decrease about $t \gtrsim 2\,(1+z)\,R/c \approx 6\,(1+z)$ years after the GRB is detected. The emission at longer wavelengths is predominantly due to cooler dust, which is further away from the GRB. The dust cloud in this model was assumed to have a maximum radius $R_\mathrm{max} = 3.67$ pc, and so the emission decreases rapidly after $t > 2\,(1+z)\,R_\mathrm{max}/c \approx 22\,(1+z)$ years. The dust emission spectrum is predicted to peak at a rest-frame wavelength of about 8 μm.

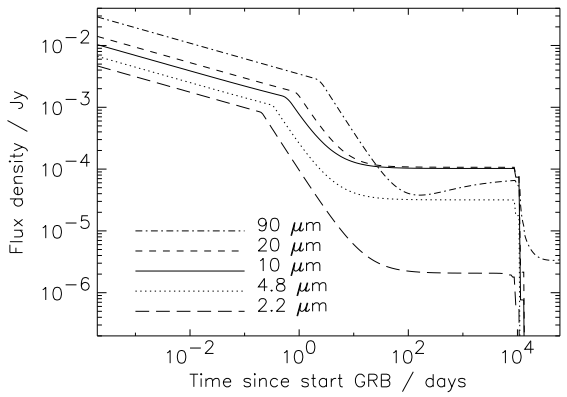

Figure 4. Emission from dust surrounding a GRB at $z = 1$, including emission from the GRB afterglow at five observed wavelengths. The light curve that heated the dust is light curve B_2 as shown in Fig. 3 (see Table 2 for its characteristics).

The dust emission predicted at the observed wavelength 170 μm at $t < 50$ days is due to the dust surrounding the GRB radiating at its original temperature in the interstellar radiation field of the GRB host galaxy, which is assumed to be 30 K. If the dust temperature assumed is different, then the flux changes by only a small factor at this wavelength. At rest-frame wavelengths longer than 100 μm, at which the spectral energy distribution of dust at 30 K peaks, there is very little excess emission due to additional heating by the GRB.

For comparison, the expected flux densities of an ULIRG similar to Arp 220 (Klaas et al. 1997), at a redshift $z = 1$, is also plotted in Fig. 3. The intensity of the emission from dust heated by the GRB at rest-frame wavelengths shorter than about 2.5 μm is expected to be less than that from starlight in such a galaxy. However, the dust emission from the GRB at wavelengths of about 5 μm can be an order of magnitude greater than the emission from the galaxy. At rest-frame wavelengths longer than about 25 μm, infrared emission from dust heated by star formation at temperatures $T \simeq 40$ K rises to dominate the spectrum. Therefore, the dust emission from a GRB within a galaxy like Arp 220 at $z = 1$ could best be observed at mid-infrared wavelengths between 5 μm and 20 μm. Note, however, that Arp 220 is a very luminous galaxy. It is likely that the host galaxy of a GRB will typically be less luminous, which would improve the observability of the GRB dust emission. Also, the infrared emission of a galaxy will be much more extended than emission from the surroundings of a GRB and could be distinguished if high spatial resolution observations were available, such as would be possible using either the Atacama Large Millemeter Array (ALMA) or a space-borne far-infrared interferometer like *SPECS* (see section 6 for more details).

5.2 The infrared GRB synchrotron afterglow

In Fig. 3 only dust emission from the environment of the GRB was plotted. However, it is likely that in the first few days after the GRB, the observed spectrum at mid-infrared wavelengths will be dominated by the GRB afterglow. In Fig. 4 the dust emission at five different wavelengths is plotted, including the emission from the GRB afterglow. The light curves of the GRB dust emission are the same as plotted in Fig. 3. It is assumed that the infrared afterglow is not attenuated by dust surrounding the GRB, however, at the shortest infrared wavelengths, dust along the line of sight could reduce the flux density of the afterglow significantly, as shown in Table 1. After a few days, the afterglow emission is decreasing as $t^{-1.375}$ (Sari et al. 1998). All the light curves shown in Fig. 4 are dominated by the afterglow in the first few weeks after the start of the GRB. After the first few weeks, the light curve flattens as the afterglow emission decreases below the level of the heated dust emission, which then dominates the light curve at late times. If the flux density of the dust emission is ten times lower than that assumed in this model, then the afterglow will dominate the spectrum for $10^{1/1.375} \approx 5$ times longer. In other less optimistic models the GRB dust emission is typically lower and so the afterglow will dominate the spectrum for a longer period.

5.3 Dust emission in various environments

The results above showed that the visibility of the optical afterglow can depend strongly on the GRB environment. Different amounts of energy are absorbed by different distributions of dust, thus influencing the infrared emission. In Fig. 5a the peak flux of the dust emission spectrum is calculated for the A-series models listed in Table 2 at $z = 1$. The maximum flux is expected to occur roughly $(1+z)$ years after the GRB is detected. The time profile of the dust emission is similar to that displayed in Fig. 3. The spectrum of the dust emission described in section 5.1 is plotted for comparison. In the case of flat dust density profiles, almost all the dust is vaporized, and so the spectrum is dominated by emission from dust near the sublimation temperature, peaking at a wavelength about $(1 + z)$ μm. In the other cases, the observed emission peaks at a longer observed wavelength close to $10\,(1 + z)$ μm.

Because the optical flash is expected to destroy a large amount of dust in the A-series light curve models, the intensity of the dust emission is less than that predicted in a model with a less luminous optical flash. This is illustrated in Fig. 5b, in which the dust emission spectrum is plotted for dust heated by the same GRB afterglow, but with an optical flash that is ten times weaker, represented by the B-series models, see Table 2. Light curve D has the same parameters as light curve B_5, except that the optical flash is this time described by a top-hat. Since in the model the total energy radiated in the optical flash is greater, more dust is destroyed and so the flux density of the dust emission is smaller. Because less dust is destroyed in the B-series models as compared with the A-series models, the intensity of the dust emission is greater in the B-series models for a given density profile.

The emission is expected to be even greater if the dust is heated by a GRB with an afterglow but no optical flash, as shown for the C-series models in Fig. 5c. If the peak luminosity of the optical flash is small, then almost no dust is destroyed and so the dust emission is intense. Except for models A_1 and A_2, for which all the dust is destroyed by the

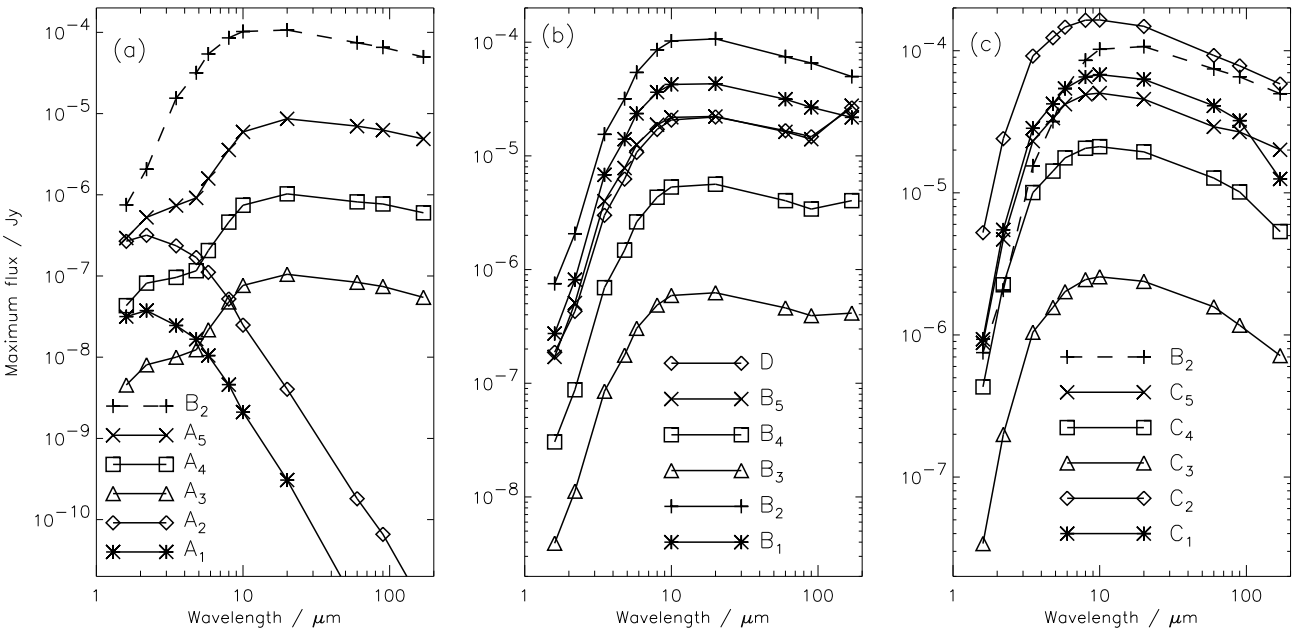

Figure 5. (a) The peak intensity of the emission spectrum of dust heated by an optical flash with $L_{\rm peak} = 10^{49}\,{\rm erg\,s^{-1}}$ and an afterglow of a GRB at $z = 1$. The dust parameters are described in Table 2. For comparison the spectrum of the more powerful dust emission in model B_2 is also plotted. (b) The peak intensity of the emission spectrum of dust heated by an optical flash with $L_{\rm peak} = 10^{48}\,{\rm erg\,s^{-1}}$ and an afterglow of a GRB at $z = 1$ in different dusty environments, described in Table 2. Curve D has the same parameters as curve B_5, except that the optical flash is not a Gaussian but a top-hat. (c) The peak intensity of the emission spectrum of dust heated by an afterglow of a GRB at $z = 1$ with no optical flash, described by parameters C_1 to C_5 in Table 2. For comparison the spectrum of the dust emission in model B_2 is also plotted.

optical flash, dust with a flat density profile emits more radiation per unit mass than dust with an isothermal profile. To obtain the greatest dust emission from a GRB, an optical flash with a low peak luminosity, a high-density environment and a flat density profile are all required.

5.4 Dust emission and the redshift of the GRB

In Fig. 6 the predicted maximum intensity of emission by dust heated by a GRB, with a model B_2 optical flash afterglow, are plotted in various bands as a function of redshift. In this optimistic model there is strong evolution with redshift: the predicted flux density decreases rapidly as the redshift increases, especially at the short wavelengths. At longer wavelengths ($\lambda \gtrsim 20\,\mu$m) the flux density decreases more slowly, as the observed wavelength approaches the peak of rest-frame spectrum.

6 OBSERVABILITY OF DUST EMISSION FROM GRBS

The observed wavelengths 3.5, 4.8, 5.8 and 8.0 μm in Fig. 6a correspond to bandpasses of the InfraRed Array Camera (IRAC) on board the *Space Infrared Telescope Facility* (*SIRTF*[†]). The Multiband Imaging Photometer for *SIRTF* (MIPS) has bandpasses at 24, 70 and 160 μm. In 1 hour of integration time, *SIRTF* could detect the near-infrared dust emission from a GRB at a redshift $z \lesssim 2$. At the longer wavelengths observable with the MIPS instrument, it is unlikely that *SIRTF* will detect dust emission from a GRB at a redshift $z \gtrsim 1$, because the emission is too weak. Also, at the longest wavelengths observable for the MIPS instrument, 70 and 160 μm, confusion noise from unresolved distant galaxies will increase the minimum detection depth, reducing the maximum redshift at which dust emission could be observable (see Blain 1999). Because the GRB dust emission at far-infrared and submillimetre wavelengths is expected to be much less intense than that at near-infrared wavelengths, facilities operating in those wavebands, like the future Stratospheric Observatory for Infrared Astronomy (SOFIA[‡]) and the *Far InfraRed and Submillimetre Telescope* (*FIRST–Herschel*[§]), are likely to be unsuccessful in detecting dust emission from high redshift GRBs. However, it should be possible to resolve the GRB dust emission using high spatial resolution facilities like ALMA[¶] and the *SPECS* (see Leisawitz et al. 1999, 2000). In cases where the optical afterglow is heavily obscured by dust and thus invisible to optical searches, ALMA could provide a very accurate position for the GRB afterglow, once the GRB position is known to within a few arcseconds. Accurate positions of

[†] Up-to-date information about SIRTF can be found at http://sirtf.caltech.edu/

[‡] see http://sofia.arc.nasa.gov/

[§] The homepage of *FIRST* is http://astro.estec.esa.nl/SA-general/Projects/First/first.html

[¶] Up-to-date information about ALMA can be found at the web page http://www.alma.nrao.edu/

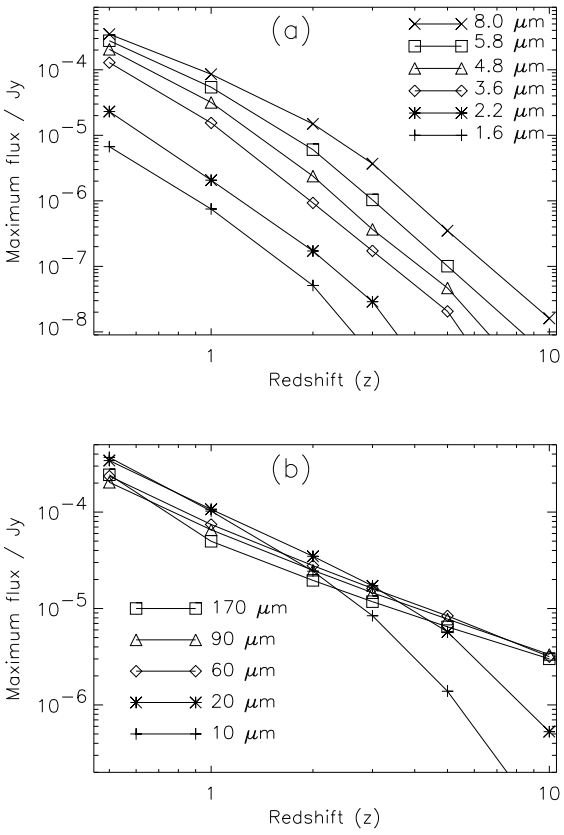

Figure 6. (a) The maximum flux density of dust emission from a GRB as a function of redshift at several different observed wavelengths model B_2. The flux density decreases rapidly as the redshift increases, between redshifts 1 and 2 the flux density decreases by a factor of about ten. The top four curves are plotted for wavelengths observable using the *SIRTF*–IRAC camera. The maximum redshifts at which the IRAC camera could detect the dust emission with a signal to noise ratio of 5 within 1 hour of integration time are 1.7, 2.1, 1.8 and 2.0 for the 3.6, 4.5, 5.8 and 8.0 bandpass respectively. (b) The maximum flux density of dust emission from the same GRB at several longer observed wavelengths. The MIPS instrument on *SIRTF* has three observing bands, at 24, 70 and 160 μm. The maximum redshifts at which MIPS could detect the dust emission with a signal-to-noise ratio of 5 within 1 hour of integration time are 0.8, 0.4 and 0.1 for the 24, 70 and 160 μm bandpass respectively. Confusion noise will limit the depth of observations at the longest wavelengths, 70 and 160 μm (Blain 1999 and references therein).

optically obscured afterglows are currently provided by the VLA at radio frequencies, as shown by Frail et al. (2000). Such accurate positions can be provided by the *Swift* satellite[‖], which will locate a GRB precisely at X-ray energies within 2.5 arcseconds (Gehrels et al. 1999). Already, a fading counterpart to a GRB with a flux density of several mJy has been detected at 850 μm (Smith et al. 1999). In a ten-minute observation ALMA will have a 5σ detection limit of about 0.2 mJy at a wavelength of 870 μm. This will be deep enough to detect the submillimetre-wave afterglow of a GRB as far away as a redshift of 10 within a day of the start of the GRB, while the afterglow of a GRB at a redshift of 5 would be detectable for three weeks.

[‖] The homepage of *Swift* with the latest updates can be found at http://swift.sonoma.edu/

7 DISCUSSION

In this paper the visibility of optical/UV GRB emission absorbed by dust and the intensities of the reprocessed radiation emitted by dust were predicted. The heating effect of GRB afterglow and prompt optical flash was calculated in a model whose parameters are consistent with the relatively sparse existing observations. A radiative transfer model was used to simulate the interaction between GRB radiation and dust grains; the temperature, opacity and sublimation rate of the dust grains in the environment of a GRB, and the infrared emission from this dust was calculated. Note that in the model the GRB emission was assumed to be isotropic and that dust destruction by X-rays was neglected. If GRBs are beamed and/or grains are predominantly destroyed by X-rays, then the dust emission as computed in the model could be reduced significantly.

The simulations showed that the visibility of the optical flash and afterglow of a GRB depends strongly on the characteristics of both the surrounding dust and the GRB emission itself. If a GRB is surrounded by a large amount of dust ($M_{\rm dust} \gtrsim 100\,{\rm M}_\odot$), then it is unlikely that an optical afterglow will be observed, unless the GRB is accompanied by a very powerful optical flash with a peak luminosity $L_{\rm peak} \gtrsim 10^{49}\,{\rm erg\,s^{-1}}$, which would destroy almost all the dust along the line of sight within a few seconds of the GRB. Because of the large-scale destruction of dust grains in this scenario, the intensity of the associated dust emission would be quite weak. If the optical flash associated with a GRB is less powerful, then less dust is destroyed. The opacity is thus higher, and so it is possible that the energy in the afterglow is almost completely absorbed, and that no late-time optical emission from the GRB would be observed. However, the reradiated energy might be detectable. In particular, the IRAC camera on *SIRTF* could detect the near-infrared dust emission in such cases out to redshifts of about 2, if the GRB could be located to within its 5−arcmin field of view. Because the light curve of this dust emission does not have any specific temporal structures, and could therefore be confused with the flux density of dust radiation from the general interstellar medium of the host galaxy, an accurate position and flux density of the GRB afterglow would need to be provided by other observations. At present these can be carried out with the VLA. In the future high-resolution submillimetre-wave observations with ALMA will be able to confirm that the origin of the infrared energy was a GRB.

A combination of observations is needed to test whether a GRB is surrounded by a large amount of dust. First of all, the lack of a detection of an afterglow in the optical waveband could be a first indication that there is a large mass of dust near the GRB. If radio observations provide an accurate position for the afterglow, then the *SIRTF* mid-infrared telescope could be used to try to detect the reprocessed dust emission directly. However, only in the most optimistic scenarios, in which more than $10^3\,{\rm M}_\odot$ of dust is present and the optical flash of the GRB is weak, is infrared emission likely

to be observed from dust heated by the optical flash and afterglow of the GRB. If either the GRB emission is beamed, or X-ray grain destruction is important, or less than $10^2\,M_\odot$ of dust surrounds the GRB, then the infrared dust emission is likely to fall below the detection limits of *SIRTF* unless the GRB is at a low redshift $z < 0.5$.

The results of the model can be compared with the results of existing observations for optical flashes from GRBs. A powerful optical flash was observed to accompany GRB990123, detected twenty seconds after the start of the GRB (Akerlof et al. 1999). From the observed redshift $z = 1.6$ (Galama et al. 1999b), the peak luminosity was calculated to be $\sim 10^{50}\,\mathrm{erg\,s^{-1}}$. This flash could easily have vaporized more than $10^3\,M_\odot$ of dust around the GRB within a few seconds. The late-time afterglow for this GRB is thus unlikely to have been attenuated by dust surrounding the GRB, and so the dust emission in this case was probably very low. Attempts to detect the prompt optical flash from other GRBs have provided only upper limits (Akerlof et al. 2000). This does not necessarily imply that the optical emission in those cases was extinguished by surrounding dust. However, if the peak luminosity of the optical flash of a GRB is well correlated with either gamma-ray fluence or gamma-ray peak flux, then in two of the observed cases the optical flash would have $L_{\rm peak} \simeq 10^{49}\,\mathrm{erg\,s^{-1}}$. This luminosity is great enough to sublime most of the surrounding dust, and thus lead to the detection of optical emission. Even if these GRBs occurred in very dusty environments, then the lack of optical emission indicates that the peak luminosity of the optical flash is probably not strongly correlated with either gamma-ray fluence or gamma-ray peak flux.

ACKNOWLEDGMENTS

We would like to thank the referee R. A. M. J. Wijers, for his helpful and useful comments, and for pointing out the X-ray dust destruction results of Fruchter et al. (2001). BPV acknowledges the support of a scholarship from the Netherlands organization for international cooperation in higher education, to study in Cambridge (Venemans 2000). AWB, Raymond and Beverly Sackler Foundation Research Fellow, thanks the Foundation for generous financial support as part of their Deep Sky Initiative Programme at the IoA.

REFERENCES

Aitken D. K., Moore T. J. T., Roche P. F., Smith C. H., Wright C. M., 1993, MNRAS, 265, L41
Akerlof C. et al., 1999, Nat, 398, 400
Akerlof C. et al., 2000, ApJ, 532, L25
Blain A. W., 1999, in Weymann R., Storrie-Lombardi L., Sawicki M., Brunner R., eds, Photometric Redshifts and the Detection of High Redshift Galaxies, ASP Conf. Ser. Vol. 191, 255, ASP, San Francisco
Bloom J. S. et al., 1999a, Nat, 401, 453
Bloom J. S. et al., 1999b, ApJ, 518, L1
Bloom J. S., Kulkarni S. R., Djorgovski S. G., 2001, AJ, submitted (astro-ph/0010176)
Cardelli J. A., Clayton G. C., Mathis J. S., 1989, ApJ, 345, 245
Costa E. et al., 1997, IAU Circ., 6572, 1
Désert F. X., Boulanger F., Puget J. L., 1990, A&A, 237, 215
Draine B. T., 2000, ApJ, 532, 273
Draine B. T., 2001, http://www.astro.princeton.edu/~draine/dust/dust.diel.html
Draine B. T., Lee H. M., 1984, ApJ, 285, 89
Esin A. A., Blandford R., 2000, ApJ, 534, L151
Evans A., 1993, The dusty universe. Wiley, New York
Frail D. A. et al., 2000, in Kippen R. M., Mallozzi R. S., Connaughton V., eds., AIP Conf. Proc. 526, Gamma-Ray Bursts: Fifth Huntsville Conference. American Institute of Physics, New York
Frail D. A. et al., 2001, Nature, submitted (astro-ph/0102282)
Fruchter A. S. et al., 1999, ApJ, 516, 683
Fruchter A. S., Krolik J. H., Rhoads J. E., 2001, preprint
Galama T. J., Wijers R. A. M. J., 2001, ApJ, 549, L209
Galama T. J. et al., 1999a, A&AS, 138, 451
Galama T. J. et al., 1999b, Nat, 398, 394
Gehrels N., Swift Science Team, 1999, BAAS, 195, 9208
Greiner J., 2001, http://www.aip.de/~jcg/grbgen.html
Groot P. J. et al., 1997, IAU Circ., 6584, 1
Guhathakurta P., Draine B. T., 1989, ApJ, 345, 230
Hanlon L. et al., 2000, A&A, 359, 941
Hildebrand R. H., 1983, QJRAS, 24, 267
Hobson M. P., Padman R., 1993, MNRAS, 264, 161
Hobson M. P., Scheuer P. A. G., 1993, MNRAS, 264, 145
Huang Y. F., Dai Z. G., Lu T., 2000, A&A, 355, L43
Katz J. I., 1994, ApJ, 432, L107
Klaas U., Haas M., Heinrichsen I., Schulz B., 1997, A&A, 325, L21
Klebesadel R. W., Strong I. B., Olson R. A., 1973, ApJ, 182, L85
Leisawitz D., Mather J. C., Moseley S. H., Xiaolei Z., 1999, Ap&SS, 269, 563
Leisawitz D., Mather J. C., Blain A. W., Langer W. D., Moseley S. H., Yorke H. W., 2000, BAAS, 197, 1409
Lamb D. Q., Castander F. J., Reichart D. E., 1999, A&AS, 138, 479
MacFadyen A. I., 2001, in Kippen R. M., Mallozzi R. S., Connaughton V., eds., AIP Conf. Proc. 526, Gamma-Ray Bursts: Fifth Huntsville Conference. American Institure of Physics, New York
MacFadyen A. I., Woosley S. E., 1999, ApJ, 524, 262
Mathis J. S., 1990, ARA&A, 28, 37
Mathis J. S., Rumpl W., Nordsieck K. H., 1977, ApJ, 217, 425
Mészáros P., Gruzinov A., 2000, ApJ, 543, L35
Mészáros P., Rees M. J., 1993, ApJ, 418, L59
Mészáros P., Rees M. J., 1997, ApJ, 476, 232
Mezger P. G., Mathis J. S., Panagia N., 1982, A&A, 105, 372
Paczynski B., 1995, PASP, 107, 1167
Perna R., Aguirre A., 2000, ApJ, 543, 56
Piran T., 1999, PhR, 314, 575
Reichart D. E., 1999, ApJ, 521, L111
Sahu K. C. et al., 1997, Nat, 387, 476
Sari R., Piran T., 1999, A&AS, 138, 537
Sari R., Piran T., Narayan R., 1998, ApJ, 497, L17
Siebenmorgen R., Krügel E., Mathis J. S., 1992, A&A, 266, 501
Smith I. A. et al., 1999, A&A, 347, 92
Sokolov V. V. et al., 2001, A&A, 372, 438
Venemans B. P., 2000, MPhil thesis, Univ. Cambridge
Waxman E., Draine B. T., 2000, ApJ, 537, 796
Witt A. N., Oliveri M. V., Schild R. E., 1990, AJ, 99, 888